Jaspinder Kaur, Roderick Melnik and Anurag Kumar Tiwari*

Forced convection heat transfer study of a blunt-headed cylinder in non-Newtonian power-law fluids

https://doi.org/10.1515/ijcre-2020-0170
Received September 8, 2020; accepted December 12, 2020; published online February 8, 2021

Abstract: In this present work, forced convection heat transfer from a heated blunt-headed cylinder in power-law fluids has been investigated numerically over the range of parameters, namely, Reynolds number (Re): 1–40, Prandtl number (Pr): 10–100 and power-law index (n): 0.3–1.8. The results are expressed in terms of local parameters, like streamline, isotherm, pressure coefficient, and local Nusselt number and global parameters, like wake length, drag coefficient, and average Nusselt number. The length of the recirculation zone on the rear side of the cylinder increases with the increasing value of Re and n. The effect of the total drag coefficient acting on the cylinder is seen to be higher at the low value of Re and its effect significant in shear-thinning fluids ($n < 1$). On the heat transfer aspect, the rate of heat transfer in fluids is increased by increasing the value of Re and Pr. The effect of heat transfer is enhanced in shear-thinning fluids up to ~ 40% and it impedes it's to ~20% shear-thickening fluids. In the end, the numerical results of the total drag coefficient and average Nusselt number (in terms of J_H–factor) have been correlated by simple expression to estimate the intermediate value for the new application.

Keywords: blunt-headed circular; drag coefficient; non-Newtonian fluids; Nusselt number; Prandtl number; Reynolds number.

***Corresponding author: Anurag Kumar Tiwari**, Department of Chemical Engineering, Dr. B. R. Ambedkar National Institute of Technology, Jalandhar 144011, Punjab, India; and MS2Discovery Interdisciplinary Research Institute, Wilfrid Laurier University, 75 University Avenue West, Waterloo N2L 3C5, ON, Canada, E-mail: tiwaria@nitj.ac.in. https://orcid.org/0000-0002-1360-1388
Jaspinder Kaur, Department of Chemical Engineering, Dr. B. R. Ambedkar National Institute of Technology, Jalandhar 144011, Punjab, India
Roderick Melnik, MS2Discovery Interdisciplinary Research Institute, Wilfrid Laurier University, 75 University Avenue West, Waterloo, N2L 3C5, ON, Canada; BCAM Basque Center for Applied Mathematics, Mazarredo Zumarkalea, 14, 48009 Bilbao, Bizkaia, Spain

1 Introduction

Forced convection heat transfer from a cylinder of different cross-sections is important not only because of its analytical or computational significance but also due to its direct and indirect connection with industrial problems related to process design calculations (Darby and Chhabra 2016; Sumer and Fredsoe 1997). In such situations, external flow past a cylinder of various geometry, reliable, and accurate information about drag and heat transfer characteristics are generally required for the process design calculations for different cross-sections of the cylinder. Another application is also found in polymeric processing operations where most of the fluids are encountered and show the behavior of the non-Newtonian fluid (Chhabra and Richardson 2011). The flow around a cylinder with different cross-section has some similarities, despite the inherent differences due to the cross-section of the cylinder, especially in terms of the presence or absence of sharp corners. Therefore, over the years, considerable research has been done to develop physical insights that are used based on improved design procedures and calculation. Hence, the bulk of information has been available on the fluid flow, heat transfer characteristics of cylinders submerged in flowing fluids stream. Also, the cylinder of different shapes (such as circular, square, elliptic, triangular, rectangular and semi-circular, etc.) has some relevance in novel heat exchangers (Hesselgreaves 2001) and other engineering process applications (Berk 2013; Chhabra 2006; Chhabra and Richardson 2011; Steinberg 1991) (like food processing, cooling of electronic components, aerosols filters, membrane separation modules, fixed beds, fluidized beds, etc.). In contrast to the circular cylinder, only limited literature is available for cylinders of non-circular cross-sections even in Newtonian fluid. Besides, there is an additional complexity arising from the orientation of a non-circular cylinder with respect to the direction of flow, types of fluids (Newtonian/non-Newtonian), nature of flow (uniform, shear, oscillating and angle of the incident for instance) and confined or unconfined flow, the aspect ratio of the cylinder and different thermal boundary condition in heat transfer. In the context of the present study, within the framework of time-independent non-Newtonian fluids, the

shear-thinning and shear-thickening viscosity, typically approximated by the power-law model, is encountered in numerous industrial settings (Chhabra 2006; Chhabra and Richardson 2011; Darby and Chhabra 2016). The power-law fluids are the class of time-independent non-Newtonian fluids which is more viscous than Newtonian fluids and flow expected to be laminar flow regime. Therefore, the flow behavior and heat transfer study in power-law fluids from the variety of shapes of bluff bodies would be different as compare to Newtonian fluids and this is due to different rheological behaviors (Chhabra, Cho, and Greene 2011). Some of the results pertinent to momentum and heat transfer from a circular cylinder in power-law fluids have been investigated numerically by researches (Bharti, Chhabra, and Eswaran 2006; Khan, Culham, and Yovanovich 2006; Soares, Ferreira, and Chhabra 2005; Zdravkovich 1997). Second most results extensive results are also available for momentum and heat transfer from an elliptic cylinder in power-law fluids studies in the laminar flow regime which is reported by Sivakumar et al. (Sivakumar, Bharti, and Chhabra 2007), Bharti et al. (Bharti, Sivakumar, and Chhabra 2008), Patel and Chhabra (Patel and Chhabra 2013). On the other hand, somewhat less extensive results for two-dimensional laminar flow studies for the semi-circular cylinder in Newtonian and power-law fluids at different orientations with respect to oncoming fluids are presented in detail (Chandra and Chhabra 2011a, b). In this study, authors are investigated momentum and heat transfer study, and the results have presented the correlation for net hydrodynamic forced, heat transfer aspects and also reported the critical Reynolds number for steady flow regime for this particular geometry. Similar but opposite orientation of semi-circular cylinder by Tiwari and Chhabra (Tiwari and Chhabra 2014) are presented numerical study for forced convection heat transfer in laminar flow range. The next study corresponds to square cylinder in power–law fluids are carried out by Paliwal et al. (Paliwal et al. 2003) in a laminar flow regime. In this study, the numerical results are presented for hydrodynamic and heat transfer part at different thermal boundary conditions, i.e., the constant heat flux and the constant wall temperature at the surface of the cylinder. Some of the studies (Pantokratoras 2016; Sahu, Chhabra, and Eswaran 2009) also show the similar dependence of drag and Nusselt number on Reynolds number and power-law index. And next configuration is a two-dimension triangular cylinder; there have been few studies on the power-law fluids flow past triangular cylinders. Prhashanna et al. (Prhashanna, Sahu, and Chhabra 2011) have elucidated the influence of the power-law index on the transitional Reynolds numbers. This study has also reported the correlation for critical Reynolds number and correlation for average Nusselt number.

In the previous study, it is clear that the momentum and heat transfer from an isotheral cylinder in power-law fluids in a unconfined domain, shear-thinning fluids behaviour can augment the rate of heat transfer up to 40 % with respect to that in Newtonian fluids whereas shear-thickening fluids behaviour impedes heat transfer by 25% under identical conditions irrespective of the flow regime. Amongst the various shapes mentioned in the preceding paragraphs, a blunt-headed cylinder (combination of semi-circular and square cylinder) has received only few attention even in Newtonian fluids Forced convective flow and heat transfer pastan unconfined blunt headed cylinder at different angles of incidence (Kapadia, Dalal, and Sarkar 2017; Pawar, Sarkar, and Saha 2020). This configuration finds industrial applications in heat exchangers design, thermal treatment of foodstuffs (e.g., beans and carrots), electronics industry and many more. This geometry also mimics some characteristics of chips in microelectronic applications, and in thermal treatment of the sliced carrots and potatoes, etc. (Berk 2013). Therefore, an adequate understanding of the underlying physics of the hydrodynamics and heat transfer phenomena of such fluid systems has been a subject of great interest to engineers and scientists for more than a century (Chhabra and Richardson 2011). Due to wide occurrence in a variety of industrial settings, very limited numerical results are available for momentum and heat transfer in power-law fluids past over an isothermal cylinder of non-circular cross-section. Furthermore, most of the studies as mention above are limited to a steady, laminar flow regime in an infinite domain. Based on the foregoing discussion, as far as according to my knowledge, there have been no previous results available for momentum and heat transfer in power-law fluids over a heated blunt-headed cylinder in the infinite domain. This work aims to fill the gap in the literature related to steady laminar flow in infinite domain studies. Therefore, the present work is reported herein are momentum and heat transfer in a steady and laminar flow regime from a two-dimensional an isothermal blunt-headed cylinder in an infinite domain. Extensive numerical results are presented in detail the streamline profiles and isotherm contour, total drag and Nusselt number, and their correlation over the ranges of conditions: power-law index: $0.3 \le n \le 1.8$; Reynolds number: $1 \le \mathrm{Re} \le 40$ and Prandtl number: $10 \le \mathrm{Pr} \le 100$. Under this certain range of dimensionless numbers, fluid flow over the cylinder is highly viscous non-Newtonian power-law fluids models and generally encountered in the process industry under the laminar flow conditions range. Therefore, it is

appropriate to consider the ranges of conditions covered in this study.

2 Problem formulation and governing equations

The flow of two-dimensional steady, incompressible power-law fluids (from left to right, at temperature T_∞) over an infinitely long heated blunt-headed cylinder at a constant wall temperature (T_w) (the geometry is composed of a semi-circular cylinder of diameter, D and a square cylinder of dimension, D) with a uniform flow velocity V_∞ is investigated numerically in an infinite domain. Due to the temperature difference ($T_w > T_\infty$), heat is being transferred from the cylinder surface to power-law fluids through the convection mode. Over the range of conditions, the thermo-physical properties of the fluid (i.e., specific heat,C_p, thermal conductivity, k, density, $\rho_\infty$and power-law parameters m and n) are assumed to be temperature-invariant over the narrow range of temperature difference (such as $\Delta T = T_w - T_\infty = 5$ K). The presence of a small value of Brinkman number (Br) is of the order of 10^{-3} and thus it is reasonably small to neglect the viscous dissipation term in the energy equation. Truly, it is very difficult the numerical simulation of the infinite flow domain. Therefore, it needs to be approximated infinite domain to an artificial circular confine domain of diameter, D_∞ for blunt-headed cylinder, as given in Figure 1(a), (b). The size of the computational domain, D_∞ is considered to be large enough to minimize the velocity and temperature boundary effects in the flow domain and also minimize the computational effort at an optimum level. Under these conditions, the governing differential equations for fluid flow and heat transfer are expressed in their dimensionless forms as follows (Bird, Stewart, and Lightfoot 2006; Tiwari and Chhabra 2014).

Continuity equation:

$$\frac{\partial V_x}{\partial x} + \frac{\partial V_y}{\partial y} = 0 \tag{1}$$

X-momentum equation:

$$\frac{\partial (V_x V_x)}{\partial x} + \frac{\partial (V_x V_y)}{\partial y} = -\frac{\partial p}{\partial x} + \frac{1}{Re}\left(\frac{\partial \tau_{xx}}{\partial x} + \frac{\partial \tau_{yx}}{\partial y}\right) \tag{2}$$

Y-momentum equation:

$$\frac{\partial (V_y V_x)}{\partial x} + \frac{\partial (V_y V_y)}{\partial y} = -\frac{\partial p}{\partial y} + \frac{1}{Re}\left(\frac{\partial \tau_{xy}}{\partial x} + \frac{\partial \tau_{yy}}{\partial y}\right) \tag{3}$$

Energy equation

$$\frac{\partial (V_x \theta)}{\partial x} + \frac{\partial (V_y \theta)}{\partial y} = \frac{1}{\mathrm{Re} \times \mathrm{Pr}}\left(\frac{\partial^2 \theta}{\partial x^2} + \frac{\partial^2 \theta}{\partial y^2}\right) \tag{4}$$

The constitutive relationship for power-law fluids, the deviatoric stress tensor, τ_{ij}, is linearly related to the shear rate tensor (or rate of deformation tensor), ε_{ij}, as follows (Bird, Stewart, and Lightfoot, 2006):

$$\tau_{ij} = 2\eta\epsilon_{ij} \tag{5}$$

Where, $\epsilon_{ij} = \frac{1}{2}\left(\frac{\partial V_i}{\partial j} + \frac{\partial V_j}{\partial i}\right)$, $i,\ j = x,\ y$.

The shear dependant viscosity η for power-law fluids is expressed as:

$$\eta = m\left(I_2/2\right)^{(n-1)/2} \tag{6}$$

In Eq. (6), m is the flow consistency index, n is the power-law index, and I_2 is the second invariant of the rate of deformation tensor. If the value of the power-law index, i.e., $n = 1$; on the other hand, $n < 1$ indicates shear-thinning fluid an $n > 1$ indicates shear-thickening fluid.

The specified boundary conditions for this present problem may be written as follows,

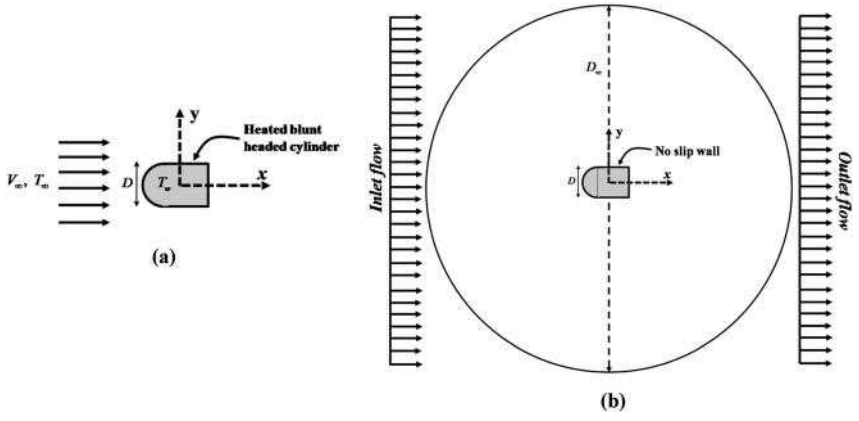

Figure 1: Schematics diagram of the unconfined flow over blunt-headed cylinder: (a) Physical model; (b) computational domain.

- The left-hand side of the artificial cylindrical part of the fluid is considered as the inlet free-stream flow condition in the x-direction is defined (i.e., $V_x = 1,\ V_y = 0,\ \theta = 0$)
- No-slip and constant wall temperature on the surface of the blunt-headed cylinder is defined (i.e., $V_x = V_y = 0,\ \theta = 1$)
- The right-hand side of the artificial cylindrical part of the fluid is considered as the outflow boundary condition (i.e., $\partial\varphi/\partial x = 0$, where $V_x,\ V_y$, and θ).

Aforementioned governing differential Eqs. (1)–(3) and applied boundary conditions are non-dimensionalized by using $D,\ V_\infty,\ \rho V_\infty^2$, and $m(V_\infty/D)^{n-1}$ scaling variables for length, velocity, pressure, and viscosity, respectively. The non-dimensional temperature is given by $\theta = (T - T_\infty/T_W - T_\infty)$ the constant wall thermal boundary conditions. After the non-dimensionalization, the dimensionless groups appearing in the governing equations, namely, Reynolds number (Re) and Prandtl number (Pr), are defined as follows:

- The *Reynolds number* (Re):

$$Re = \frac{\rho_\infty V_\infty^{2-n} D^n}{m} \tag{7}$$

- The *Prandtl number* (Pr):

$$Pr = \frac{C_p m}{k}\left(\frac{V_\infty}{D}\right)^{n-1} \tag{8}$$

The governing differential Eqs. (1)–(4) with the appropriate boundary conditions have been solved numerically to get the solution inflow domain in terms of the velocity, pressure and temperature fields over wide ranges of physical and kinematic parameters. These, in turn, are used to express the results in terms of hydrodynamics characteristics, as listed below:

- The surface pressure coefficient:

$$C_P = \frac{p_s - p_\infty}{\frac{1}{2}\rho V_\infty^2} \tag{9}$$

where p_s is the local pressure on the cylinder and p_∞ is pressure away from the cylinder.

- The total drag coefficient:

$$C_D = \frac{F_D}{\frac{1}{2}\rho V_\infty^2 D} = C_{DP} + C_{DF} \tag{10}$$

where F_D is the total drag force acting on the cylinder per area. On can express the total drag coefficient into the individual drag coefficients, C_{DP} and C_{DF} which can be evaluated using the following definitions:

$$C_{DP} = \frac{F_{DP}}{\frac{1}{2}\rho V_\infty^2 D} = \int_S C_p n_x dS \tag{11}$$

$$C_{DF} = \frac{F_{DF}}{\frac{1}{2}\rho V_\infty^2 D} = \frac{2^{n+1}}{\mathrm{Re}}\int_S (\tau \cdot n_s) dS$$
$$= \frac{2^{n+1}}{\mathrm{Re}}\int_S (\tau_{xx} n_x + \tau_{xy} n_y) dS \tag{12}$$

where F_{DP} and F_{DF} is the pressure component and frictional component of the total drag force and S is the surface area and unit vector, n_s, normal to the surface of the cylinder.

In the heat transfer analysis, the local value Nusselt number on the surface of the blunt-headed cylinder is expressed in terms of the non-dimensional temperate normal to the surface which is defined as:

$$Nu = \frac{hD}{k} = -\left(\frac{\partial\theta}{\partial n_s}\right) \tag{13}$$

where n_s is the unit normal vector on the surface of the cylinder, If one can integrate the local values of Nusselt number over the surface of the cylinder to obtain the average value of Nusselt number which is evaluated as follows,

$$Nu_{avg} = \frac{1}{S}\int_S Nu\ dS \tag{14}$$

In summary, fluid flow analysis: recirculation length, pressure coefficient on the surface of the cylinder and net hydrodynamic force in terms of total drag coefficient are expected to be depended by the power-law index (n) and Reynolds number (Re) whereas the heat transfer analysis shows the additional influence on the Prandtl number (Pr). This present work aims to develop the relationship between the parameter over a wide range of conditions to the steady flow regime.

3 Numerical solution procedure

The governing partial differential (Eq.(1)–(4)) for momentum and heat transfer from a blunt-headed cylinder along with the specified boundary conditions have been solved numerically based on commercial software COMSOL Multiphysics® (Finite element based solver) (Patel and Chhabra 2013; Tiwari and Chhabra 2014). A two-dimension (2D), time-independent, symmetric, and laminar single-phase fluid flow module was selected with an additional physics of heat transfer in fluids. Since detailed numerical descriptions of the solution methodology used here are similar to some of our studies available elsewhere (Tiwari

and Chhabra 2014, 2015), only the key points are highlighted here. The non-uniform triangular mesh with fine grid cells was created near the surface of the heated cylinder to resolve the steep gradients (velocity and temperature), the grid expansion ratio was made progressively coarse as away from the cylinder using suitable values of the successive ratio. The Lagrangian P_2–P_1 scheme was used for the pressure and velocity fields. The **PARDISO** was employed to solve the discretized governing differential equations. In the parametric solver, the Reynolds number, Re, and power-law index, n, are used as a parametric sweep. Due to the nonlinear characteristics of the power-law fluids model, the nonlinear (Newton's) method is used to increase the convergence rate of the numerical solution. To get rid of convergence problems, the solution was always initiated using the converged Newtonian flow ($n = 1$) for given values of Re and Pr. The relative convergence criterion order of 10^{-5} for both momentum and energy equations was used (Roache 1998) the value of global parameters such as the drag and Nusselt number had also stabilized at least up to four significant digits within the convergence criterion.

4 Choice of numerical parameters

The detailed description of the domain and grid independence test is not repeated here because it has been already given in a previous computational study (Bharti, Chhabra, and Eswaran 2006; Bharti, Sivakumar, and Chhabra 2008; Chandra and Chhabra 2011a, b; Prhashanna, Sahu, and Chhabra 2011; Roache 1998; Sivakumar, Bharti, and Chhabra 2007; Tiwari and Chhabra 2014). In this present study, as the computational domain is changed from $D_\infty/D = 100$ to $D_\infty/D = 150$, very little variation is observed in global parameters (such as total drag and average Nusselt number) as indicated in Table 1. Therefore, the value of computational domain, $D_\infty/D = 100$ is used as a optimum domain size with 320 number of grid points on the surface of the blunt-headed cylinder and 51,760 total number of elements in the computational domain. Next, three non-uniform computational grids (G1, G2, G3, Table 2) are created to investigate the effect of grids size to select an optimum grid for the present problem. The grid independence studies are summarized (in Table 2) in terms of the resulting value of total drag and average Nusselt number. The value of total drag coefficient and average Nusselt number changes by about ~2% between G2 to G3 but it required more computational effort. Therefore, the grid G2 is identified to be sufficient for the present computational study. To add further results to verify the grid test, Figure 2 compare the results of grid G2 and G3 in terms of surface pressure coefficient, both results are indistinguishable from each other. The detailed examination of the numerical results is presented in Table 2 and Figure 2 and it is suggested that grid G2 is our optimum grid to resolve the thin momentum and thermal boundary layers near the surface cylinder. Therefore, the results reported in the present study are based on $D_\infty/D = 100$ and grid, G2.

Table 1: Domain independence test at Re = 1 and Re = 40.

D_∞/d	Re = 1					
	C_D			Nu_{avg}		
	$n = 0.3$	$n = 1.0$	$n = 1.8$	$n = 0.3$	$n = 1.0$	$n = 1.8$
40	25.607	13.020	7.2886	5.2566	1.3719	0.4864
50	25.183	12.635	7.0497	5.1747	1.3611	0.4835
60	24.876	12.387	6.9011	5.1150	1.3543	0.4819
D_∞/d	Re = 40					
	C_D			Nu_{avg}		
	$n = 0.3$	$n = 1.0$	$n = 1.8$	$n = 0.3$	$n = 1.0$	$n = 1.8$
40	1.2210	1.6253	1.8266	37.837	6.7512	1.7347
50	1.2166	1.6119	1.8036	37.634	6.7346	1.7308
60	1.2140	1.6041	1.7912	37.504	6.7241	1.7288

To verify the assumption which we have considered in this study, the steady laminar flow regime over the given range of parameters. Therefore, the transient numerical simulation of governing differential equations has been solved using the time depended solver in the full computational domain at the maximum value of Re = 40, Pr = 100, for the extreme value of the power-law index, $n = 0.3$ and $n = 1.8$, the resulting velocity and temperature fields were found to be steady and symmetric with respect to the x-axis of the flow domain and the corresponding numerical values of drag and Nusselt number were obtained to be indistinguishable with the assumptions of the steady laminar flow regime. After that, the validity of the present numerical results is verified by a few comparisons with the literature results in our next section Table 3.

5 Results and discussion

The numerical results embracing wide ranges of dimensionless parameters, Reynolds number ($1 \le \mathrm{Re} \le 40$), Prandtl number ($10 \le \mathrm{Pr} \le 100$), and power-law index ($0.3 \le n \le 1.8$) for momentum and heat transfer in steady laminar flow were obtained to elucidate the effect on

Table 2: Grid independence test at Re = 40 and Pr = 100.

Grid	No. of elements	N_P	C_D			Nu_{avg}		
			$n = 0.3$	$n = 1.0$	$n = 1.8$	$n = 0.3$	$n = 1.0$	$n = 1.8$
G1	38,406	251	1.2151	1.6055	1.7949	230.09	15.720	3.6649
G2	42,668	299	1.2140	1.6041	1.7912	184.60	15.544	3.6623
G3	46,816	343	1.2137	1.6050	1.7939	153.74	15.407	3.6631

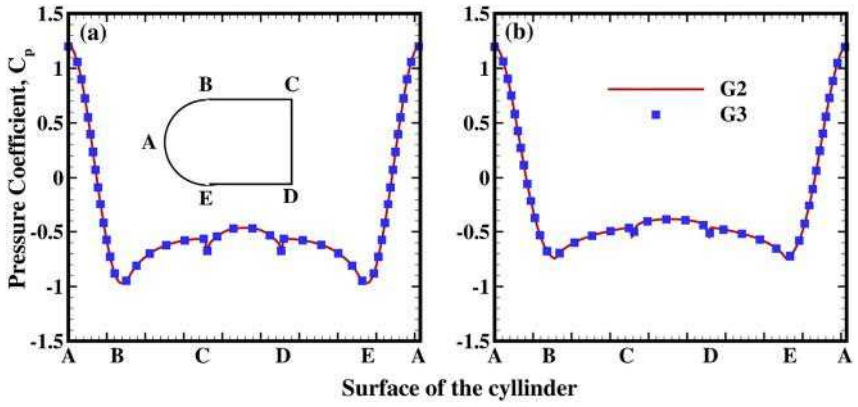

Figure 2: Surface pressure coefficient for grid independence test at Re = 40 (a) $n = 0.3$, (b) $n = 1.8$. The grid G2 and G3 represented by the dot and line symbol respectively.

Table 3: Validation with semicircular cylinder (curved face oriented upstream) in the steady flow regime.

Re	n	Present		Ref (Chandra and Chhabra 2011a, b)		Ref (Chatterjee and Mondal 2015)	
		C_D	L_r	C_D	L_r	C_D	L_r
10	0.2	3.112	0.484	3.009	0.488	–	–
	1.0	2.706	0.817	2.710	0.822	2.712	0.837
	1.8	2.561	1.648	2.532	1.658	–	–
30	0.2	1.440	1.998	1.432	2.013	–	–
	1.0	1.702	2.372	1.691	2.374	1.645	2.375
	1.8	1.815	4.044	1.807	4.073	–	–

streamline, isotherm contours near the surface of the cylinder, recirculation length and pressure coefficient whereas the global characteristics are defined in terms of the drag coefficient and Nusselt number. However, before going to detail presentation of the results, it is important to ascertain the reliability and accuracy of present numerical results obtained in the work.

5.1 Validation of results

As noted earlier, no prior numerical results are available in the literature for the present geometrical configuration investigated over the range of parameters for the power-law fluids model. Therefore, the reliable results of analogous geometry are used for validation numerical results. The first validation results are shown in Table 1 and that are related to the semi-circular cylinder in a steady flow regime. The corresponding maximum difference for total drag coefficient and recirculation length in power-law fluids with Chandra and Chhabra (Chandra and Chhabra 2011a, b) is ~2 and ~1%, respectively. The corresponding deviations for Newtonian fluids are of the order of ~3% from that of Chatterjee et al. (Chatterjee and Mondal 2015). Next, reliable numerical results of a square cylinder are available for validation of the second benchmark problem. Figure 3 represents the validation results in terms of total drag coefficient for square cylinder and a fair agreement with Okajima et al. (Okajima 1990), Sharma and Eswaran (Sharma and Eswaran 2004) and Dong-Hyeog et al. (Dong-Hyeog, Kyung-Soo, and Choon-Bum 2010) are obtained. These results differ from each other by ~3% and a fair agreement is evident. Furthermore, the comparison for present numerical results with the available data and correlation from previous studies related to the long circular cylinder (L/D>>1) and this constitutes the benchmark problem related to heat transfer. Figure 4 shows validation with an empirical model for average Nusselt number proposed by Ahmed and Yovanovich (Ahmed and Yovanovich 1995), one observed at low Reynolds number, there is a significant difference and this is due to the effect of L/D, the

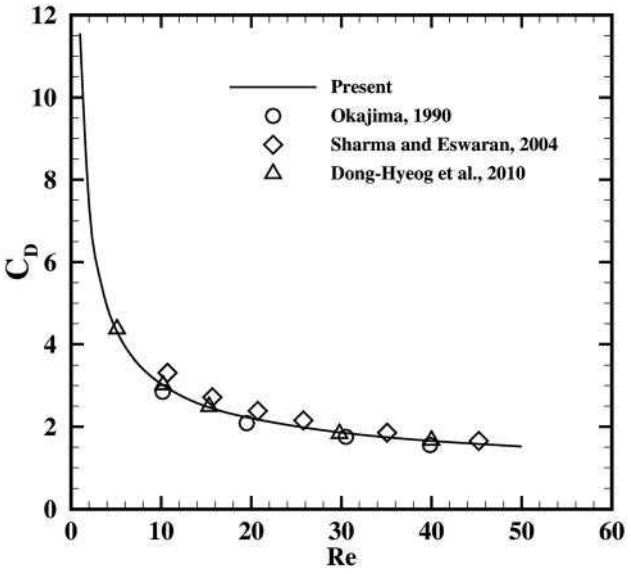

Figure 3: Results of total drag coefficient results vs. Reynolds number for Newtonian fluids (n = 1) for square cylinder. Symbols represent the results of literatures and the present results are shown by lines.

maximum deviation ~ 25% at low Re (Re < 10) and ~ 6% for high Re (Re ≥ 10). Figure 4 also shows comparisons for average Nusselt number with the correlations predicted by Churchill and Bernstein (Churchill and Bernstein 1977), Louis and Howard (Vessot and Howard 1914), and Hilpert (Hilpert 1933). Discrepancies of ~4–7% are observed with the results of Kings (Vessot and Howard 1914) and Hilpert

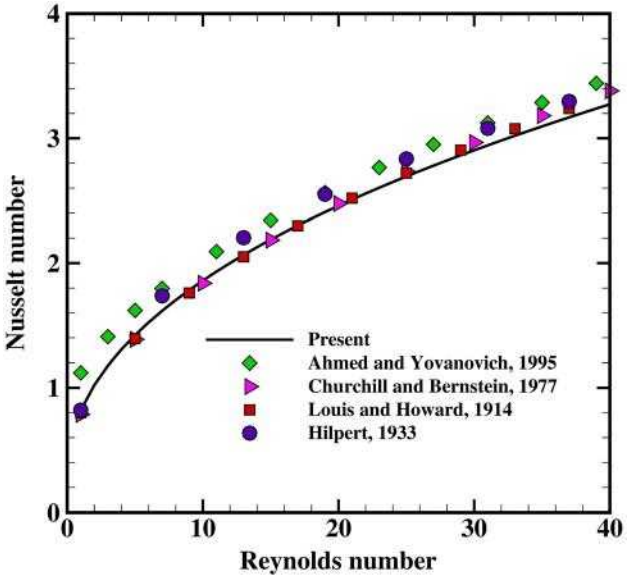

Figure 4: Results of average Nusselt number for Newtonian fluids (n = 1 and Pr = 0.71) for square cylinder. Symbols represent the results of literatures and the present results are shown by lines.

(Hilpert 1933) while our results are good agreements with that of Churchill and Bernstein (Churchill and Bernstein 1977). Such deviation from the present numerical results is ascribed due to the differences in domains and grids, solution methodology (finite element, finite difference or finite volume), convergence criterion, etc. (Roache 1998). These comparisons show that the present numerical study is in good agreement with most of the previous studies which are close to the present configuration. Based on the aforementioned validation results together with our previous experience, the present numerical results are expected to be reliable up to ~4–5%.

5.2 Streamline profiles and recirculation length

The variation of streamline profiles near the blunt-headed cylinder is dependent on the value of Reynolds's number and power-law index, as shown in Figure 5. At low values of the Reynolds number (e.g., Re = 1), the effect of viscous forces dominant the flow as compared to inertial forces, the fluid element follows the shape of the cylinder in the direction of flow without much loss in its momentum. In this case, the effect of the power-law index on streamline profiles are visualized at three value of n = 0.3, n = 1.0 and n = 1.8, no flow separation is observed up to $n \leq 1$ whereas the flow separation is observed for $n > 1$, such as n = 1.8. For instance, at low values of Re = 1, no flow separation is observed up to $n \leq 1$ whereas the flow separation is observed for $n > 1$, such as n = 1.8 (see in Figure 5).

As the Reynolds number increases up to the intermediate value (e.g., Re = 20), the influence of inertial forces increases as compare to viscous forces where an adverse pressure gradient is established at a fixed corner point of the cylinder which leads to flow separation on the rear side of the cylinder flow and separation bubble grows in the direction of flow for all value of the power-law index. For instance, Re = 20, the wake size is seen on the rear side of the cylinder but the wake region is seen to be smaller in size at this Reynolds number for shear-thinning fluid (n = 0.3), in contrast to Newtonian and shear-thickening fluids. This is also observed in literature where the same kind of behaviors was predicted (Chandra and Chhabra 2011a, b; Dhiman, Chhabra, and Eswaran 2006; Prhashanna, Sahu, and Chhabra 2011). At the extreme value of Re = 40, a well develop wake region has been observed in both shear-thinning-fluids, n = 0.3, and shear-thickening fluids, n = 1.8 (Figure 5(d), (h)). The wake region grows in size as the value of the power-law index is gradually changed from

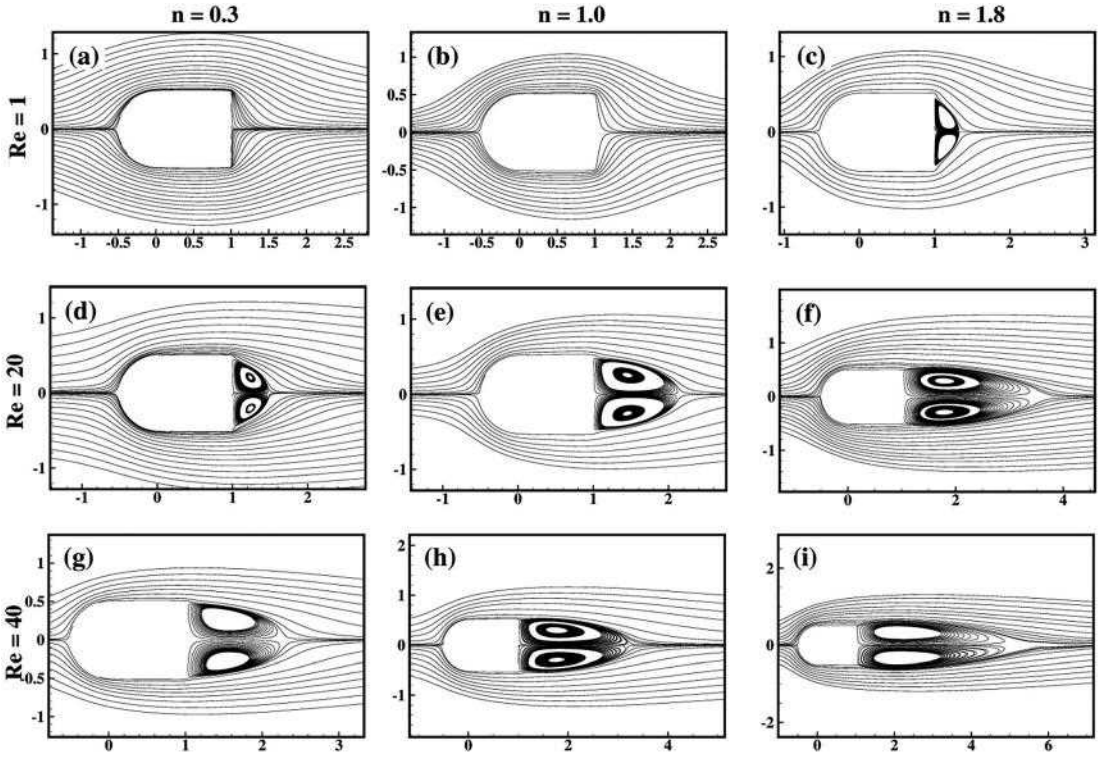

Figure 5: Variation of streamlines profiles near the surface of the blunt-headed cylinder.

shear-thickening fluids to shear-thinning-fluids irrespective of Reynolds's number.

On the other hand, the variation of the wake size in terms of the dimensionless recirculation length, as a function of Reynolds number and power-law index are shown in Figure 6. It can be seen that at a fixed value of the power-law index, the wake size gradually increases as the Reynolds number increases due to the gradual dominance of the inertia forces over the viscous forces. The size of the recirculation zone is also increasing with increasing value of the power-law index, irrespective of Reynolds's number. Furthermore, the influence of the Reynolds number on the recirculation length is seen to be more pronounced than that of the power-law index. This result obtained in the present study qualitatively similar to 2-D shape bodies like cylinders of circular and non-circular cross-sections (Chandra and Chhabra 2011a, b; Dhiman, Chhabra, and Eswaran 2006; Prhashanna, Sahu, and Chhabra 2011; Tiwari and Chhabra 2014). The present numerical results of dimensionless recirculation length are correlated by the following expression,

$$L_r = 0.053\mathrm{Re}^{1.32} + 4.67\left(\frac{n}{n+1}\right)^{7.52} \quad (15)$$

Equation (15) correlates the present numerical data over the range of dimensionless parameter with an average error of 4.3% which rises to a maximum of 13.4%.

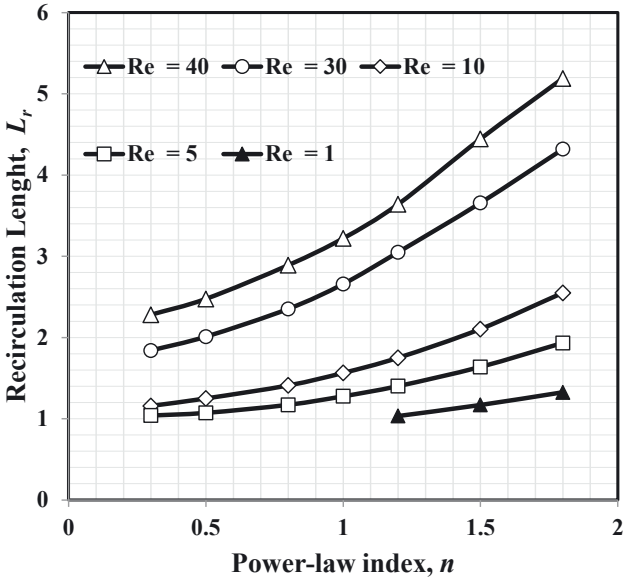

Figure 6: Variation of recirculation length (L_r) with Reynolds number (Re) and power-law index (n).

5.3 Surface pressure coefficient

Look at the further insights into the resulting hydrodynamic forces on the surface of the cylinder that can be examined in terms of the pressure distribution on the

surface of the blunt-headed cylinder. Since the flow is steady and symmetry over the range of parameters considered here, therefore the variation of the surface pressure coefficient (C_P) on only half part of the cylinder is sufficient for the explanation, as shown in Figure 7. The variation of C_P on the surface of the cylinder is expected to be dependent on Reynolds number (Re) and power-law index (n) (e.g., $C_P = f(\mathrm{Re}, n)$). The value C_P is plotted on the surface of the blunt-headed cylinder (a-b-c-d) for four representative values of the Re = 1, 10, 30, and 40 and for three values of n = 0.3, 1.0 and 1.8. The variation C_P is a strong function of n at low Re and its value decreases as the value of n changes from shear-thinning ($n < 1$) to shear-thickening ($n > 1$). As we can see in the figure, at low Re (e.g., Re = 1), the magnitude of C_P decreases with increasing value of n, the variation of C_P maximum at the front stagnation point a and decreases along the front curve surface (a-b) of the cylinder, after that it is attained almost constant variation along the horizontal surface (b-c) then reached to the corner point c (geometrical singularity points) and after that increases along the vertical surface of the cylinder (c-d). The variation C_P is seen to be reversed in the rear side of the cylinder with the value of n. The values of C_P on the surface of the cylinder decreases with the increased value of the Reynolds number (e.g., Re = 10, 30, and 40) at the fixed value of the power-law index. The variation C_P is seen to increase with increasing value of n and this trend completely reverse after point b on the surface of the cylinder when the Reynolds number, Re > 10. This non-monotonic variation of the C_P possibly expects from the interaction between two terms which is present in the hydrodynamic equations, namely, the viscous and inertial forces. Furthermore, the effect of n is seen to be strong in shear-thinning fluids ($n < 1$) with the increasing value of the Reynolds number.

5.4 Drag phenomena

The net hydrodynamics force are experienced by the blunt headed cylinder in terms of total drag coefficient in the direction of flow. Figure 8 (a) represents functional dependency of the total drag coefficient (C_D) with Reynolds number (Re) and power-law index (n). For a fixed value of n, the value of C_D always displays the well-known inverse type of relationship with Re, i.e., C_D always decreases as values of the Re increases. For instance, at fixed value of power-law index (at n = 1.0), the value of C_D decreases from 12.387 to 1.604 as the value of Re increases from Re = 1 to Re = 40. On the other hand, the dependency of C_D decreases with increasing value of n at the fixed value of Re. As the value of Re increases from Re = 1 to Re = 40, the value of C_D decreases by 23.67, 10.78, and 5.11 for n = 0.3, n = 1.0, and n = 1.8, respectively. It is seen that the C_D contributes significantly in shear-thinning ($n < 1$)

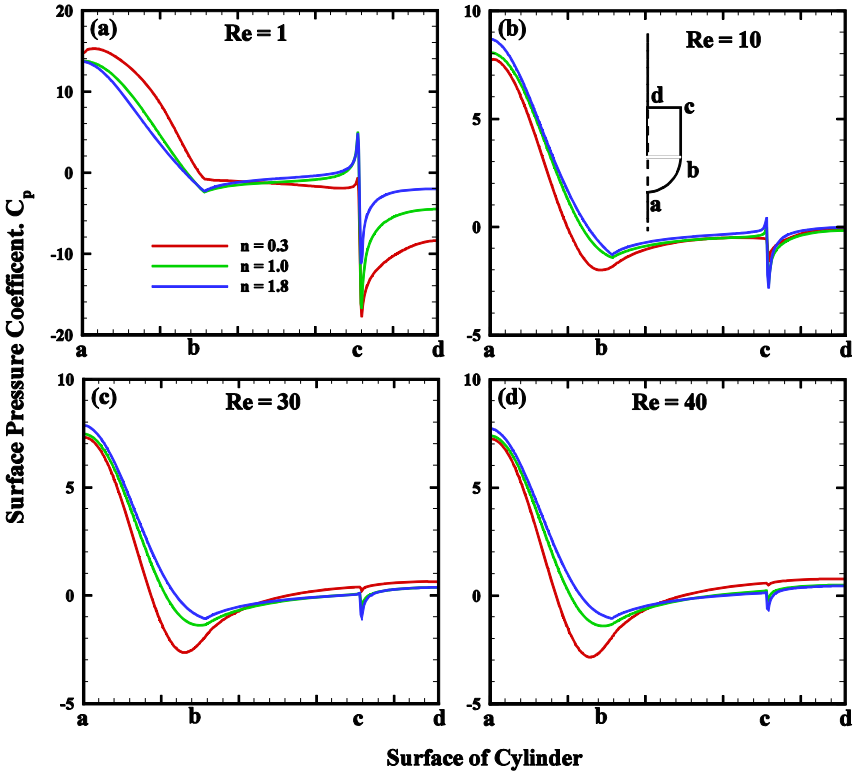

Figure 7: Distribution of the pressure coefficient on the surface of a blunt-headed cylinder (half-part).

and Newtonian fluids (n = 1) whereas this contribution is small in shear-thickening fluids (n > 1). Similar kind of observations are also found in literature for circular (Bharti, Chhabra, and Eswaran 2006; Bharti, Chhabra, and Eswaran 2007a, b; Sivakumar, Prakash Bharti, and Chhabra 2006), elliptic (Bharti, Sivakumar, and Chhabra 2008; Rao, Sahu, and Chhabra 2010; Sivakumar, Bharti, and Chhabra 2007) and semi-circular (Chandra and Chhabra 2011a, b; Gupta, Ray, and Chatterjee 2014; Pal Singh Bhinder, Sarkar, and Dalal 2012; Tiwari and Chhabra 2014) cylinders. Further, look into the relative contributions of the individual drag coefficients to the total drag coefficient can be examining the dependency of the ratio (C_{DP}/C_{DF}) with Re and n, as shown in Figure 8 (b). This ratio is seen to always increase with the increase with Re and decreasing with n. For instance, at Re = 40, the value of this ratio is ~2.57 in a shear-thinning fluid (n = 0.3) and ~ 0.95 in a shear-thickening fluid (n = 1.8) whereas ~1.326 in Newtonian fluids (n = 1). The effect of this ratio (C_{DP}/C_{DF}) is changed very small with Re in the case of Newtonian fluid whereas its value is higher in lower shear-thinning fluids behavior (n < 1). This is clearly shown that the C_{DP} always contributes a significant portion to the C_D as compared to C_{DF}, especially in shear-thinning fluids (n < 1) whereas the contribution of viscous component progressively increases with the increasing degree of shear-thickening behavior (n > 1). This is also consistent with the scaling argument of the viscous forces as $\sim V_\infty^{\,n}$ and the inertial force as $\sim V_\infty^{\,2}$. Also, from simple dimensional arguments, one can expect that the ratio of (C_{DP}/C_{DF}) will approximately vary as $\sim V_\infty^{\,-1}$ in the case of Newtonian fluid and therefore, viscous forces decrease with the increasing value of the Re. On the other hand, for power-law fluid, the ratio of (C_{DP}/C_{DF}) is expected to vary as $\sim V_\infty^{n-2}$ and thus, this ratio shows a stronger dependence on velocity for shear-thinning fluids (n < 1) than that for shear-thickening fluids (n > 1). Finally, from an application point of view, the present results of drag coefficient are approximated by using a simple correlation through a non-linear regression analysis over the range of conditions as follows,

$$C_D = \frac{a}{\mathrm{Re}}\left(1 + bn\mathrm{Re}^{(cn+d)}\right), \tag{16}$$

The best fitted values of the four parameters are: a = 26.693, b = −0.473, c = 0.064 and d = −0.578. Equation (16) reproduces the present numerical data (139 data points) with average and maximum deviations of 9.29 and 26.49%.

5.5 Isotherm contours near the cylinder

It is customary to visualize the temperature profile in terms of the isotherm contours, especially near the heated cylinder. Such plots are shown a qualitative behavior of thermal boundary layer thickness and also the determination of the "hot" and "cold" regions nearby cylinder and that is required during the thermal processing of temperature-sensitive materials. Figure 9 depicted the isotherm contours near the surface of the cylinder, at two different values Pr = 10 and Pr = 100 for three values of Re = 1, 20, and 40, three values of n = 0.3, 1.0, and 1.8. In this figure, it is seen that at a fixed value of the power-law index, at low Reynolds number, for instance, Re = 1, the isotherm contour follow the shape of the cylinder and less dense near the surface of the cylinder which indicates the weak temperature gradient normal to the cylinder surface. This is simply because the advection is very weak, and heat transfer occurs by conduction only. However, with the increasing value of Reynolds number, the crowding of isotherm contours near the surface of the cylinder is seen to occur due to the flow separation happening at high-value Reynolds number (such as Re = 20 and 40). In this case, the value of the Peclet number (Pe = Re × Pr) increases and this can lead to the thinning of the thermal boundary layer which crowded the isotherms contour near the cylinder. For Newtonian fluids (n = 1), the boundary layer thickness represents a stronger dependence on the Reynolds number (scale as ~ $\mathrm{Re}^{-1/2}$) than that on the Prandtl number (scale as ~ $\mathrm{Pr}^{-1/3}$). Furthermore, at fixed values of n and Re, one

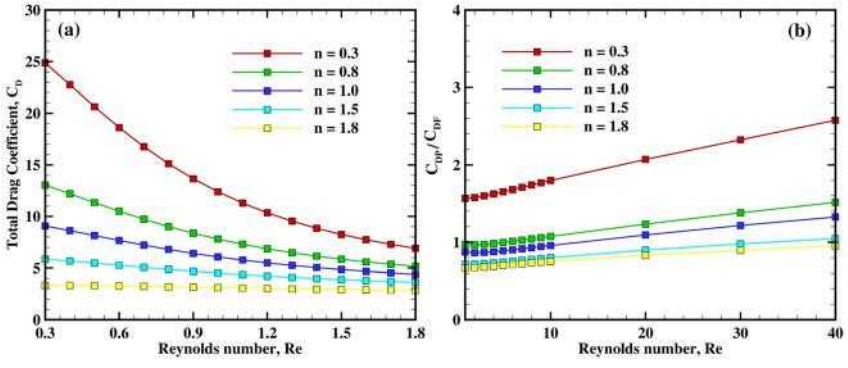

Figure 8: (a) Representation of total drag coefficient (C_D) with power-law index (n) and Reynolds number (Re), (b) Variation of C_{DP}/C_{DF} with power-law index (n) and Reynolds number (Re).

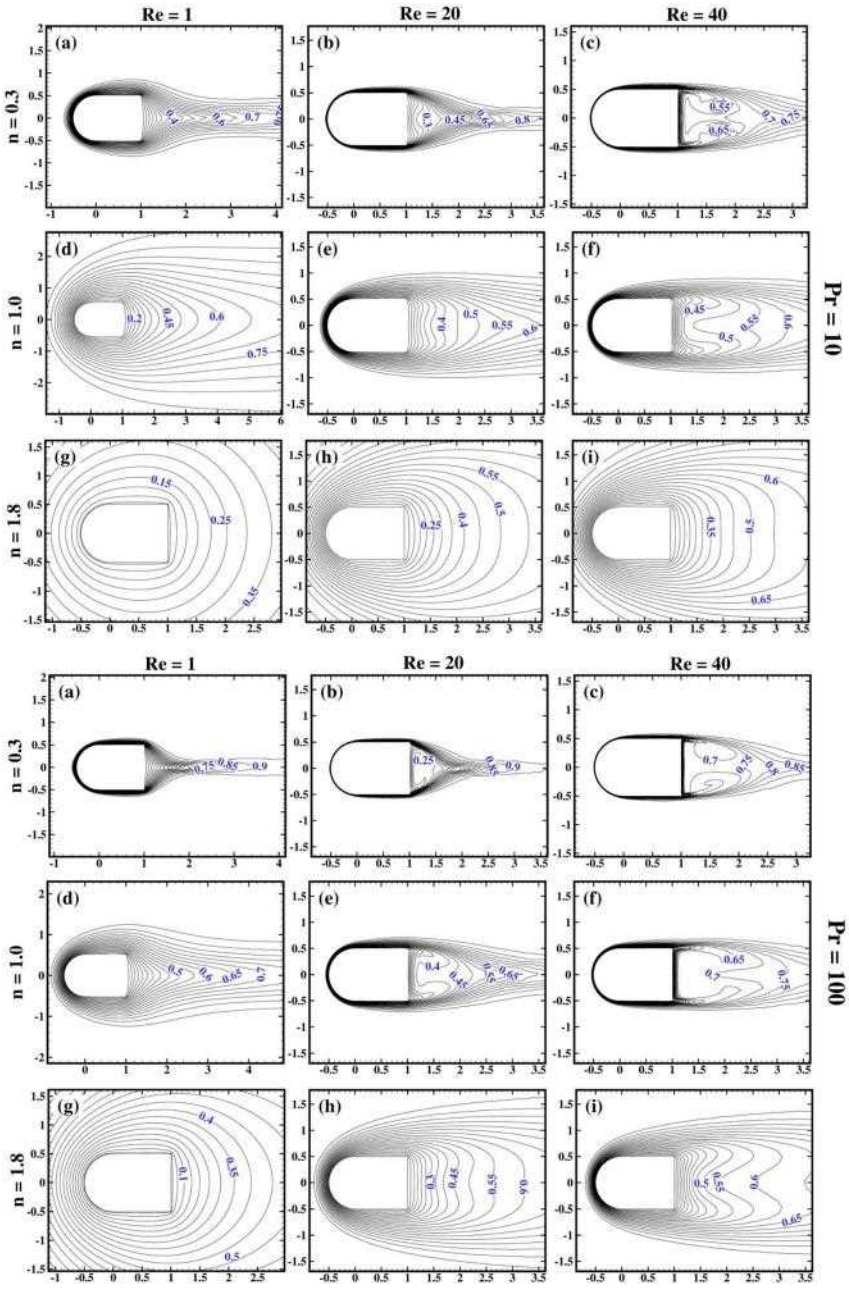

Figure 9: Variation of isotherm contours in the vicinity the blunt-headed cylinder.

would expect that as the Peclet number (Pe = Re × Pr) can be increased by increasing the value of the Prandtl number (Pr = 10 to 100). This increasing value of Pr is seen to be thinning the thermal boundary layer which leads to crowding of isotherms at the front-rear surface of the cylinder. Therefore, one can expect the gradual increment in heat transfer with progressively increasing the value of the Prandtl number. Irrespective of Reynolds number and Prandtl number, the effect of boundary layer thickness is accentuated in the case of shear-thinning fluids ($n < 1$) due to the crowding of isotherm contours as compare to Newtonian ($n = 1$) and shear-thickening fluids ($n > 1$). For instance, at Re = 40 the isotherm contours are more crowded in shear-thinning fluids, $n = 0.3$ as compared to shear-thinning fluids, $n = 1.8$. Hence, one would anticipate some enhancement in heat transfer in shear-thinning fluids and, of course, some impediments of the heat transfer in shear-thickening fluids.

5.6 Variation of local Nusselt number

The local convective heat transfer characteristics have defined by the local value of Nusselt number as expressed

in Eq. (13). Since the flow is symmetric and steady within the range of parameters considered here, only half part of the computational domain is sufficient for the explanation. The combined effect of dimensionless parameters such as Reynolds number (Re), Prandtl number (Pr), and power-law index (n) on the local value of Nusselt number is shown in Figure 10. At low values of Re or Pr or both, irrespective of n, the maximum value of local Nusselt number occurs somewhere between the point A (front stagnation point) and B (see at Re = 1, Pr = 10 or Pe = 10). This is simply so due to weak advection current and heat transfer occurs mainly by conduction. This behavior is seen in Figure 10. However, as the value of the Re or Pr or both greatly increase (e.g., Re = 40 or Pr = 100 or Pe = 4000), the magnitude of Nu increases with decreasing the thermal boundary layer in the presence of strong advection current. On the other hand, as the flow behavior of fluids changes from shear-thinning (n = 0.3, Figure 10(a)) to shear-thickening (1.8, Figure 10(g)) via Newtonian fluids (n = 1, Figure 10(d)), the maximum values of the Nu is shifted at the front stagnation point A on the surface of the cylinder at a fixed value of Re and Pr where the temperature gradient is maximum at this point. At the singularity points C (at the corner of the cylinder) the Nusselt number goes through a sudden jump in its magnitude, after that it returns to point D of the cylinder. Moreover, one can also explain this behavior by recognizing the fact that the rate of thinning of the hydrodynamic and thermal boundary layers are represented different dependences on the power-law index and their dependency on power-law index appears in the definitions of both Reynolds number (see Eq. (10)) and Prandtl numbers (see Eq. (11)). Notwithstanding this complexity stemming from the non-linear fluid behavior of power-law fluids. Broadly speaking, the rate of heat transfer shows a positive function on the Re and Pr and inverse dependence of n. The detailed dependency of parameters on the average value of the Nusselt number is presented in the following section.

5.7 Average Nusselt number

In engineering applications, the calculation of average Nusselt number (Nu_{avg}) is frequently needed in thermal treatment in any processes industry. The functional dependency of Nu_{avg} with Reynolds number (Re), Prandtl

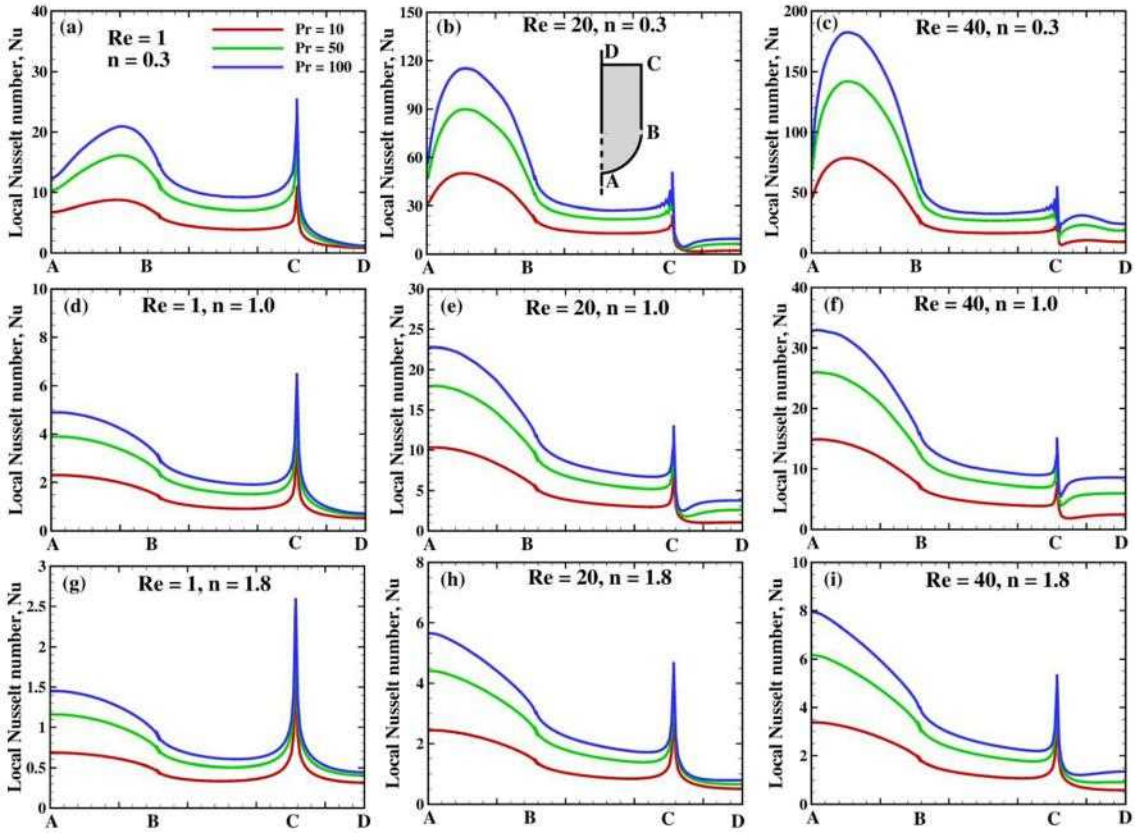

Figure 10: Distribution of the local Nusselt number (Nu) along the surface of the blunt-headed cylinder

number (Pr), and power-law index (n) is shown in Figure 11 (a)–(c). The detailed examination of results shows that the value of Nu_{avg} exhibits positive dependence on both Re and Pr irrespective of the value of the n. This aspect is also consistent as per the scaling behaviours, $Nu_{avg} \sim Re^{1/2}$ and $Nu_{avg} \sim Pr^{1/3}$ respectively.

Furthermore, the value of Nu_{avg} being shown the nonlinear dependency with power-law index (n) which is increases with the decreasing value of n. It is clearly seen that due to the reduction in effective viscosity of fluids in the vicinity of the cylinder and therefore the rate of heat transfer from the cylinder increases. For instance, at a constant value of Re = 40 and Pr = 10, as the value of the power-law index decreases from n = 1 to 0.3, the value of Nu_{avg} increased by ~41.33%. On the other hand, as the value of the power-law index increases from n = 1 to 1.8, the value of Nu_{avg} decreases by ~25.71%. The corresponding values of Nu_{avg} at Re = 40 and Pr = 100 is ~ 45.84% and ~23.57%, respectively. It is expected from the results, the shear-thinning behavior can promote the rate of heat transfer whereas the shear-thickening behavior has impeded the effect. This result is also consistent with that literature results for other shapes of the cylinder such as circular, square in the steady flow regime. Furthermore, all else being equal, it can be concluded that shear-thinning fluid behavior promotes heat transfer by up to ~ 40% in comparison to that in Newtonian fluids under appropriate conditions.

Finally, it is useful to develop the correlate the present numerical results of Nu_{avg} for engineering application, in terms of the dependent parameters, namely, Re, Pr, and n. Therefore, the present numerical results have been correlated by introducing the Colburn j_H–factor defined as

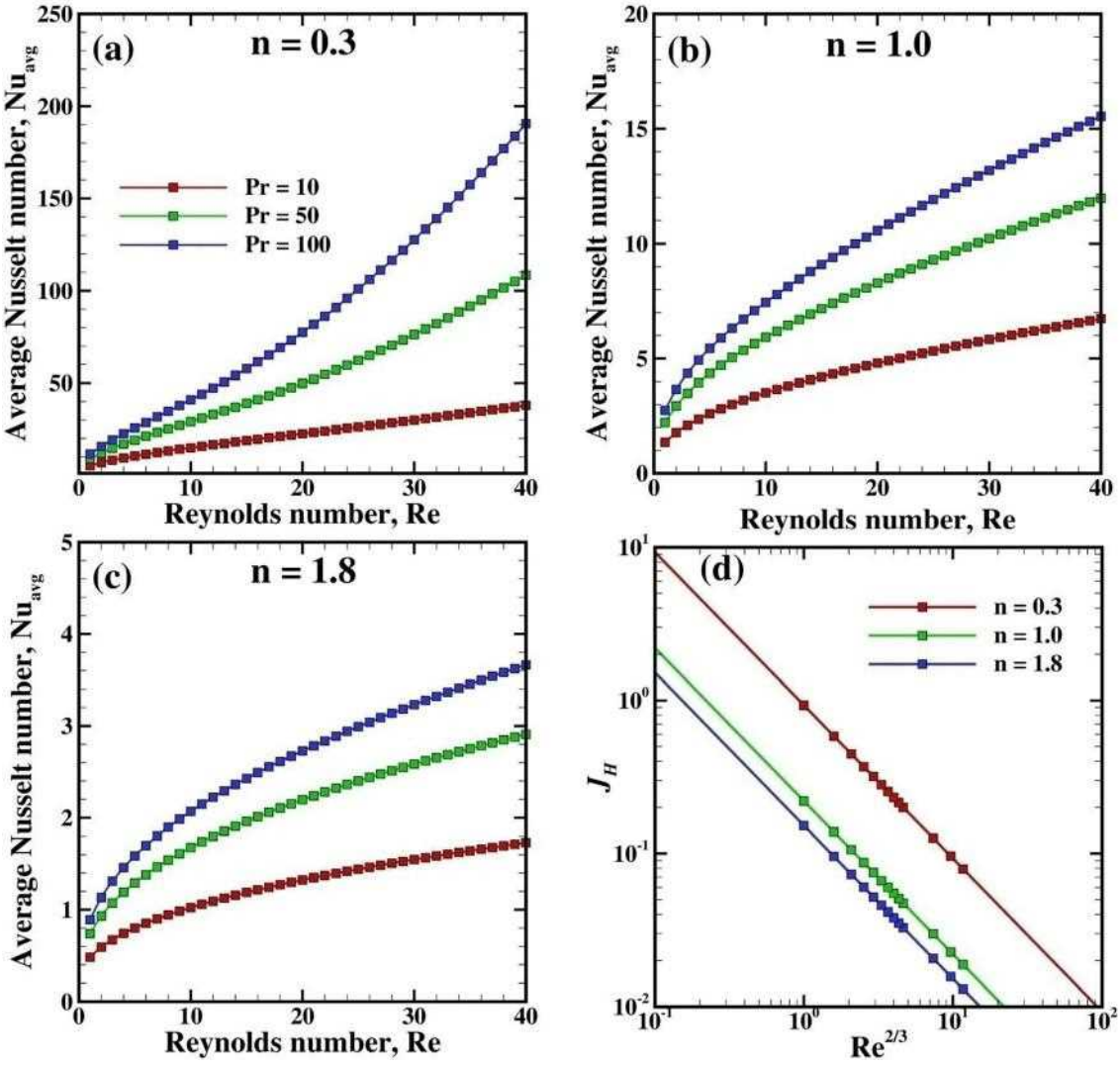

Figure 11: Results of average Nusselt number vs. Reynolds number for power-law index, (a) n = 0.2, (b) n = 1, (c) n = 1.8 and (d) dependence of j_H–factor with Reynolds number (Re) and power-law index (n).

$$j_H = \frac{Nu_{avg}}{\mathrm{Re} \times \mathrm{Pr}^{1/3}} = \left(\frac{0.22}{\mathrm{Re}^{2/3}}\right)\left(\frac{3n+1}{4n}\right)^{3.135}, \quad (17)$$

In Eq. (17), the present numerical results correlated with 320 data points, the average and maximum error of ~9.29%, and 24.81% respectively. Furthermore, Eq. (17) consistent with the scaling argument with Prandtl number, $Nu_{avg} \sim \mathrm{Pr}^{1/3}$ as well as for $j_H \sim \mathrm{Re}^{2/3}$ as shown in Figure 11 (d). On the other hand, the positive dependency of the term $((3n+1)/4n)$ in Eq. (17) also captures the shear-thinning behavior in heat transfer analysis which can be used in energy process applications.

In the end, it is worthwhile to recall here the most important assumption in the present work is that constant thermo-physical property. Among all the thermo-physical properties, power-law consistency index (m) shows the strongest temperature dependence, it is necessary to modify Eq. (17) to account this aspect by using the correction factor $(m_b'/m_w')^{0.14}$ (Chhabra and Richardson 2011). In future work, we will systematically investigated the temperature depended consistency index.

6 Conclusion

The two-dimensional forced convection heat transfer from an isothermal blunt-headed cylinder in power-law fluids in an infinite domain has been studied numerically over the range of parameters: Reynolds number (Re): 1–40, Prandtl number (Pr): 10–100 and power-law index (n): 0.3–1.8. The extensive numerical results of hydrodynamic characteristics are expressed in terms of velocity fields and recirculation lengths, total drag coefficient, pressure, and friction drag coefficients. The heat transfer characteristics are presented in terms of isotherm contour, local Nusselt number, and average Nusselt number. The hydrodynamics results are expressed as: the variation of recirculation length increases with the Reynolds number and power-law index (n). The total drag coefficient is shown the classical inverse relationship with the Re and this behavior is more prominent in shear-thinning fluids behaviors at low value of Re. On the other hand heat transfer results: the heat transfer characteristics are shown the positive dependence with Re and Pr whereas the effect of Reynolds number is stronger. The effect of the power-law index on heat transfer results, shear-thinning fluids behavior ($n < 1$) increases the rate of heat transfer up to ~40% and shear-thickening fluids behavior ($n > 1$) impedes the rate of heat transfer approximately 20% from the cylinder. In the end, the present numerical results of total drag coefficients and average Nusselt numbers are correlated via a simple expression that can be used in the calculation of the new engineering process application.

Nomenclature

Br	Brinkman number (dimensionless)
C_D	drag coefficient (dimensionless) $\left(=\frac{2F_D}{\rho_\infty V_\infty^2 D}\right)$
C_{DF}	frictional component of drag coefficient (dimensionless) $\left(=\frac{2F_{DF}}{\rho_\infty V_\infty^2 D}\right)$
C_{DP}	pressure component of drag coefficient (dimensionless) $\left(=\frac{2F_{DP}}{\rho_\infty V_\infty^2 D}\right)$
C_p	thermal heat capacity of fluid (J kg^{-1} K^{-1})
D	diameter of cylinder (m)
D_∞	diameter of computational domain (m)
F_D	drag force per unit length of the cylinder (N m^{-1})
F_{DF}	frictional component of drag force per unit length of the cylinder (N m^{-1})
F_{DP}	pressure component of drag force per unit length of the cylinder (N m^{-1})
g	acceleration due to gravity (m s^{-2})
h	heat transfer coefficient (W m^{-2} K^{-1})
I_2	second invariant of the rate of the deformation tensor, (s^{-2})
j_H	Colburn factor (dimensionless)
k	thermal conductivity of fluid (W m^{-1} K^{-1})
L_r	recirculation length (dimensionless)
m	power-law consistency index (Pa s^n)
m_b'	apparent consistency index at bulk temperature of the fluids (Pa s^n)
m_w'	apparent consistency index at wall temperature (Pa s^n)
n	power-law index (dimensionless)
n_s	unit normal vector
Nu	local Nusselt number (dimensionless)
Nu_{avg}	average Nusselt number (dimensionless)
p	pressure (Pa)local surface pressure (Pa)
Pr	Prandtl number (dimensionless)
p	pressure (Pa)local surface pressure (Pa)
Re	Reynolds number (dimensionless)
S	surface area of cylinder (m^2)
T	temperature of fluid (K)
T_∞	inlet temperature of fluids (K)
T_w	wall temperature at the surface of the cylinder (K)
Δ	temperature difference (K) (= $T_w - T_\infty$)
V_∞	free stream velocity at the inlet (m s^{-1})
V_x, V_y	x- and y-components of velocity (m s^{-1})

Greek symbols

ε	rate of strain tensor (s^{-1})
η	non-Newtonian viscosity (Pa s)viscosity of the fluid (Pa.s)
ρ	density of fluid (kg m^{-3})
ρ_∞	density of fluid at the reference temperature (kg m^{-3})
φ	dependent variable, V_x, V_y, and θ
θ	fluids temperature (dimensionless)
η	non-Newtonian viscosity (Pa s)viscosity of the fluid (Pa.s)
τ	extra stress tensor (Pa)

Subscripts

x, y, i, j	cartesian coordinates (m)
s	surface of the cylinder
∞	free stream condition at the inlet

Author contribution: All the authors have accepted responsibility for the entire content of this submitted manuscript and approved submission.
Research funding: None declared.
Conflict of interest statement: The authors declare no conflicts of interest regarding this article.

References

Ahmed, G. R., and M. Yovanovich. 1995. "Analytical Method for Forced Convection from Flat Plates, Circular Cylinders, and Spheres." *Journal of Thermophysics and Heat Transfer* 9 (3): 516–23.

Berk, Z. 2013. *Food Process Engineering and Technology*. Elsevier Science.

Bharti, R. P., R. P. Chhabra, and V. Eswaran. 2006. "Steady Flow of Power Law Fluids across a Circular Cylinder." *The Canadian Journal of Chemical Engineering* 84 (4): 406–21.

Bharti, R. P., R. P. Chhabra, and V. Eswaran. 2007a. "A Numerical Study of the Steady Forced Convection Heat Transfer from an Unconfined Circular Cylinder." *Heat and Mass Transfer* 43 (7): 639–48.

Bharti, R. P., R. P. Chhabra, and V. Eswaran. 2007b. "Steady Forced Convection Heat Transfer from a Heated Circular Cylinder to Power-Law Fluids." *International Journal of Heat and Mass Transfer* 50 (5): 977–90.

Bharti, R. P., P. Sivakumar, and R. P. Chhabra. 2008. "Forced Convection Heat Transfer from an Elliptical Cylinder to Power-Law Fluids." *International Journal of Heat and Mass Transfer* 51 (7): 1838–53.

Bird, R. B., W. E. Stewart, and E. N. Lightfoot. 2006. *Transport Phenomena*. John Wiley & Sons.

Chandra, A., and R. P. Chhabra. 2011a. "Flow over and Forced Convection Heat Transfer in Newtonian Fluids from a Semi-circular Cylinder." *International Journal of Heat and Mass Transfer* 54 (1): 225–41.

Chandra, A., and R. P. Chhabra. 2011b. "Influence of Power-Law Index on Transitional Reynolds Numbers for Flow over a Semi-circular Cylinder." *Applied Mathematical Modelling* 35 (12): 5766–85.

Chatterjee, D., and B. Mondal. 2015. "Effect of Thermal Buoyancy on Fluid Flow and Heat Transfer across a Semicircular Cylinder in Cross-Flow at Low Reynolds Numbers." *Numerical Heat Transfer, Part A: Applications* 67 (4): 436–53.

Chhabra, R. P. 2006. *Bubbles, Drops, and Particles in Non-Newtonian Fluids*. CRC Press.

Chhabra, R. P., Y. I. Cho, and G. A. Greene. 2011. *Fluid Flow and Heat Transfer from Circular and Noncircular Cylinders Submerged in Non-Newtonian Liquids, Advances in Heat Transfer*. Elsevier.

Chhabra, R. P., and J. F. Richardson. 2011. *Non-Newtonian Flow and Applied Rheology: Engineering Applications*. Elsevier Science.

Churchill, S. W., and M. Bernstein. 1977. "A Correlating Equation for Forced Convection from Gases and Liquids to a Circular Cylinder in Cross-Flow." *Journal of Heat Transfer* 99 (2): 300–6.

Darby, R., and R. P. Chhabra. 2016. *Chemical Engineering Fluid Mechanics*. CRC Press.

Dhiman, A. K., R. P. Chhabra, and V. Eswaran. 2006. "Steady Flow of Power-Law Fluids across a Square Cylinder." *Chemical Engineering Research and Design* 84 (4): 300–10.

Dong-Hyeog, Y., Y. Kyung-Soo, and C. Choon-Bum. 2010. "Flow Past a Square Cylinder with an Angle of Incidence." *Physics of Fluids* 22 (4): 043603.

Gupta, S. K., S. Ray, and D. Chatterjee. 2014. "Forced Convection Heat Transfer in Power-Law Fluids Around a Semicircular Cylinder at Incidence." *Numerical Heat Transfer, Part A: Applications* 67 (9): 952–71.

Hesselgreaves, J. E. 2001. *Compact Heat Exchangers: Selection, Design and Operation*. Elsevier Science.

Hilpert, R. 1933. "Wärmeabgabe von geheizten Drähten und Rohren im Luftstrom." *Forschung auf dem Gebiet des Ingenieurwesens A* 4 (5): 215–24.

Kapadia, H., A. Dalal, and S. Sarkar. 2017. "Forced Convective Flow and Heat Transfer Past an Unconfined Blunt Headed Cylinder." *Numerical Heat Transfer, Part A: Applications* 72 (5): 372–88.

Khan, W. A., J. R. Culham, and M. M. Yovanovich. 2006. "Fluid Flow and Heat Transfer in Power-Law Fluids across Circular Cylinders: Analytical Study." *Journal of Heat Transfer* 128 (9): 870–8.

Okajima, A. 1990. "Numerical Simulation of Flow Around Rectangular Cylinders." *Journal of Wind Engineering and Industrial Aerodynamics* 33 (1): 171–80.

Pal Singh Bhinder, A., S. Sarkar, and A. Dalal. 2012. "Flow over and Forced Convection Heat Transfer around a Semi-circular Cylinder at Incidence." *International Journal of Heat and Mass Transfer* 55 (19): 5171–84.

Paliwal, B., A. Sharma, R. P. Chhabra, and V. Eswaran. 2003. "Power Law Fluid Flow Past a Square Cylinder: Momentum and Heat Transfer Characteristics." *Chemical Engineering Science* 58 (23): 5315–29.

Pantokratoras, A. 2016. "Steady Flow of a Power-Law Non-newtonian Fluid across an Unconfined Square Cylinder." *Journal of Applied Mechanics and Technical Physics* 57 (2): 264–74.

Patel, S. A., and R. P. Chhabra. 2013. "Steady Flow of Bingham Plastic Fluids Past an Elliptical Cylinder." *Journal of Non-Newtonian Fluid Mechanics* 202: 32–53.

Pawar, A. P., S. Sarkar, and S. K. Saha. 2020. "Forced Convective Flow and Heat Transfer Past an Unconfined Blunt Headed Cylinder at Different Angles of Incidence." *Applied Mathematical Modelling* 82: 888–915.

Prhashanna, A., A. K. Sahu, and R. P. Chhabra. 2011. "Flow of Power-Law Fluids Past an Equilateral Triangular Cylinder: Momentum and Heat Transfer Characteristics." *International Journal of Thermal Sciences* 50 (10): 2027–41.

Rao, P. K., A. K. Sahu, and R. P. Chhabra. 2010. "Flow of Newtonian and Power-Law Fluids Past an Elliptical Cylinder: A Numerical Study." *Industrial & Engineering Chemistry Research* 49 (14): 6649–61.

Roache, P. J. 1998. *Verification and Validation in Computational Science and Engineering*. Hermosa Publishers.

Sahu, A. K., R. P. Chhabra, and V. Eswaran. 2009. "Two-dimensional Unsteady Laminar Flow of a Power Law Fluid across a Square Cylinder." *Journal of Non-Newtonian Fluid Mechanics* 160 (2): 157–67.

Sharma, A., and V. Eswaran. 2004. "Heat and Fluid Flow across a Square Cylinder in the Two Dimensional Laminar Flow Regime." *Numerical Heat Transfer, Part A: Applications* 45 (3): 247–69.

Sivakumar, P., R. P. Bharti, and R. P. Chhabra. 2007. "Steady Flow of Power-Law Fluids across an Unconfined Elliptical Cylinder." *Chemical Engineering Science* 62 (6): 1682–702.

Sivakumar, P., R. Prakash Bharti, and R. P. Chhabra. 2006. "Effect of Power-Law Index on Critical Parameters for Power-Law Flow across an Unconfined Circular Cylinder." *Chemical Engineering Science* 61 (18): 6035–46.

Soares, A. A., J. M. Ferreira, and R. P. Chhabra. 2005. "Flow and Forced Convection Heat Transfer in Crossflow of Non-newtonian Fluids over a Circular Cylinder." *Industrial & Engineering Chemistry Research* 44 (15): 5815–27.

Steinberg, D. S. 1991. *Cooling Techniques for Electronic Equipment*. Wiley.

Sumer, B. M., and J. Fredsoe. 1997. *Hydrodynamics around Cylindrical Structures*. World Scientific.

Tiwari, A. K., and R. P. Chhabra. 2014. "Momentum and Heat Transfer Characteristics for the Flow of Power-Law Fluids over a Semicircular Cylinder." *Numerical Heat Transfer, Part A: Applications* 66 (12): 1365–88.

Tiwari, A. K., and R. P. Chhabra. 2015. "Mixed Convection in Power-Law Fluids from a Heated Semicircular Cylinder: Effect of Aiding Buoyancy." *Numerical Heat Transfer, Part A: Applications* 67 (3): 330–56.

Vessot, L. K., and B. T. Howard. 1914. "On the Convection of Heat from Small Cylinders in a Stream of Fluid: Determination of the Convection Constants of Small Platinum Wires, with Applications to Hot-Wire Anemometry." *Proceedings of the Royal Society of London. Series A, Containing Papers of a Mathematical and Physical Character, Royal Society*: 563–70.

Zdravkovich, M. M. 1997. *Flow around Circular Cylinders: Volume I: Fundamentals*. Oxford: OUP.